Utilizing 1D FMCW Radar Data for Distance Estimation to Port Infrastructure

Mirjam Bogner, Fynn Pieper, Christian Steger, Matthias Steidel, Janusz A. Piotrowski, Sebastian Feuerstack
German Aerospace Center (DLR), Institute of Systems Engineering for Future Mobility
Escherweg 2, 26121 Oldenburg, Germany
Email: {mirjam.bogner, fynn.pieper, christian.steger, matthias.steidel, janusz.piotrowski, sebastian.feuerstack}@dlr.de

***Abstract*—Assistance systems play an important role in the proceeding transition of surface vessels towards highly automated operations. Particularly when navigating through congested areas like harbors, exact knowledge of distances to nearby obstacles is essential for collision avoidance. This paper applies a combined filtering and clustering approach in order to utilize 1D FMCW radar data for distance estimation to nearby obstacles in the harbor environment. The data processing aims at clearing the raw sensor data from unwanted signals caused by environmental influences like rain or waves and determines a reliable distance from the relevant signals. We evaluate our approach using sea trial data from a research vessel, comparing processed radar distances with a DGPS-based ground truth. The study assesses the performance of three density-based clustering algorithms – DBSCAN, HDBSCAN, and OPTICS – in this context.**

All of these algorithms show a good performance for processing the 1D FMCW data for our use case, enabling a reliable distance determination to a static obstacle. OPTICS performs slightly better in terms of eliminating disturbing signals than the remaining two algorithms. The processing times of all algorithms were found to be sufficient for online application of the proposed approach.

***Index Terms*—FMCW radar, sea trial, clustering, automated shipping, collision avoidance**

I. Introduction

The maritime industry is on the way of transitioning from manual navigation to highly automated ships. The International Maritime Organization's (IMO) framework [1] defines four levels of automation, ranging from semi-automated to fully autonomous. A Maritime Autonomous Surface Ship (MASS) at the highest level (Level 4) requires no human intervention for navigation [2].

The increasing stages of automation require enhanced sensor and assistive technologies since awareness of other participants and static obstacles is indispensable for safe operation, especially in congested waterways. In this context, several challenges for sensor readings have to be mastered that are unique or more pronounced in the maritime environment with respect to other domains. Ship movements, characterized by six degrees of freedom, can lead to distortions in sensor data. Additionally, common maritime conditions include reflections from waves on the water surface which can create deceptive signals, a problem emphasized in [3]. Heavy rainfall or fog, an issue also faced by the automotive and aviation domains, can further complicate environment perception. These factors can result in the incorrect identification of nearby objects, leading to false alarms in assessing collision risks. In the face of these challenges and potential technical failures, it is advisable to rely on redundant sensor systems for collision avoidance in automated navigation. Common technologies employed in collision avoidance systems for Maritime Autonomous Surface Ships include Cameras (e.g. [4]) and Light Detection and Ranging (LiDAR, e.g. [5], [6]), along with nautical radars. Due to their resolution and operating range, the latter are not well-suited for object detection in short distances. Instead, they are employed for ship to ship collision avoidance, as proposed e.g. by [7]. For this reason, 1-dimensional Frequency-Modulated Continuous-Wave (1D FMCW) radars appear as a viable solution for complementing collision avoidance technologies with a short-range solution capable of operating in limited visibility conditions.

Since this kind of sensors is applied in the industrial [8], [9] and aviation sectors [10], they are available as serial products and offer a good cost effectiveness, which suggests benefits also from an application in the maritime domain.

Due to the above-mentioned environmental influences, data processing of raw distances measured by the 1D FMCW radar sensors is crucial for eliminating disturbing signals. Therefore, this contribution aims at comparing the performance of three density-based clustering algorithms in utilizing 1D FMCW radar data for distance estimation to port infrastructure. The distance values are evaluated against a DGPS-based ground truth. The processing time of the proposed approach is also considered.

The data processing has been tested in sea trials with radar sensors mounted on a research boat, as depicted in Fig. 1. The maneuver performed included a head-on approach to the

Fig. 1. 1D FMCW radar sensor mounted at the bow of our research boat.

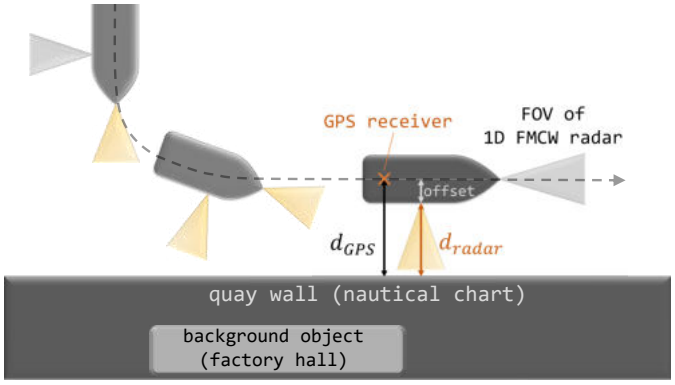

Fig. 2. Schematic illustration of the sea trial maneuver used for evaluating the data processing of the 1D FMCW radar data. The image is explained in detail in Sect. IV in the context of our evaluation methodology.

quay, followed by a 90° starboard turn and finally a phase were the vessel was moving parallel to the quay. The executed maneuver is illustrated in Fig. 2, which will be explained in detail in Sect. IV that is dedicated to the methodology of our evaluation. The use case for the evaluation was derived in the context of the AMISIA[1] project, which aims at developing a concept for a highly automated hopper dredger. The maneuver is prototypical for a hopper dredger that has to maintain the harbor area and therefore operates in close distance to the quay wall.

II. State of the Art

Radars have been used for a long time to improve safety in the automotive domain [11]. They are applied for example in park assist, blind spot assist and adaptive cruise control systems. While in the beginning the main task was to support humans in their decision-making process, radar-based assistance systems have been further developed into fully automated systems. This technology is not only employed to protect the passengers of the car from accidents but also vulnerable road users like pedestrians or cyclists [12].

In this context, applying a density-based clustering algorithm is a common means to group signal detections together to form objects. One clustering algorithm that has been applied to process radar data in several studies in the Automotive Domain (e.g. [13], [14], [15]) is Density-Based Spatial Clustering of Applications with Noise (DBSCAN) [16]. The core principle of DBSCAN is to group closely packed data points into clusters while labeling outliers as noise. It operates based on two primary input parameters: ϵ, which defines the neighborhood radius around each data point, and *min_samples*, specifying the minimum number of points required in the neighbourhood of a core point. If there is a lower number of points within the search radius, the corresponding data points are classified as noise.

Its capability of noise removal qualifies DBSCAN for applications in scenarios with high noise, as evidenced by Lim et al. [13], who effectively employed DBSCAN in adaptive cruise control systems. Scheiner et al. [14] filter their radar data in a first processing step by density and radial velocity. Then, they apply a slightly modified version of DBSCAN which eliminates extraneous radar reflections.

Among the general caveats of DBSCAN is its sensitivity to the choice of ϵ and *min_samples*. Since ϵ imposes a global density threshold, the algorithm is not suited to detect clusters of varying densities. Hierarchical DBSCAN (HDBSCAN) [17] aims at overcoming this issue by providing a hierarchical clustering approach. It performs density based clustering over a range of ϵ values and returns the cluster distribution that is most consistent over varying ϵ. Therefore, it has a better ability to form clusters in data sets of varying densities. This is particularly beneficial in radar applications where signals from targets with different geometries and reflectivity at varying distances from the sensor have to be clustered. As an additional parameter with respect to DBSCAN, a *min_cluster_size* can be defined for HDBSCAN, which is the minimum total number of data points required to form a cluster.

Another density-based clustering technique is Ordering Points To Identify the Clustering Structure (OPTICS) [18]. Like HDBSCAN, it does not use a single ϵ parameter. Instead, OPTICS sorts the data points based on their reachability distance within the data space. Similar to HDBSCAN, OPTICS can identify clusters with different densities and shapes.

III. Processing of our 1D FMCW Radar Data

To the best of our knowledge, none of the radar data processing approaches presented in Sect. II have been applied to 1D FMCW radar data in the maritime environment. Based on the mentioned studies, a combined filtering and clustering approach was selected with the aim to utilize 1D FMCW radar data for distance estimation in the maritime environment. The main objective of the data processing is first eliminating irrelevant signals and then determining a reliable distance to a static obstacle from the remaining measurements.

DBSCAN is the density-based clustering algorithm that is most frequently applied in radar data processing in the literature. As mentioned above, HDBSCAN and OPTICS are expected to better cope with clusters of varying densities, which are likely to occur in a dynamic environment. Therefore, the performance of DBSCAN, HDBSCAN and OPTICS in processing our radar data is compared. All three algorithms have the capability of outlier removal, which means that sea clutter and scattered signals can be classified as noise and filtered out. Also, they don't require *a priori* knowledge of the number of clusters, which is necessary for other algorithms, such as K-means clustering. Since the radar sensors have to detect objects in a changing field of view, the number of clusters is not known in advance.

Fig. 3 gives a schematic overview over the processing steps involved, which are explained in detail in the following sections. Data points recorded during a time interval of 1 s are considered in each processing step, i.e. 10 radar measurements are processed together since the sensors conduct 10

[1]Advanced Port Maintenance: Intelligent, Sustainable, Innovative and Automated Dredging

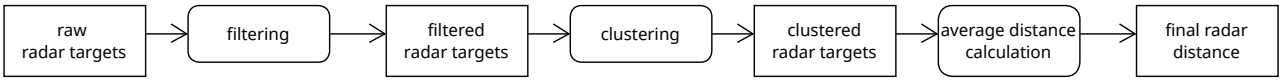

Fig. 3. Activity diagram of our data processing approach.

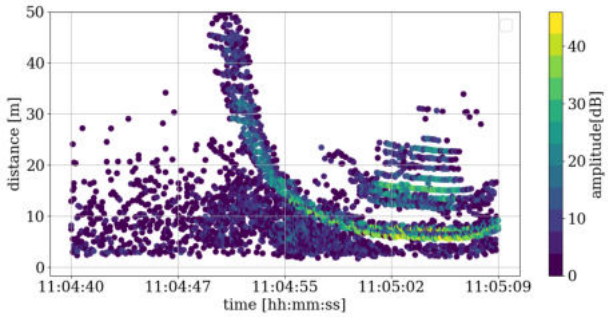

Fig. 4. Radar reflections recorded during rain. The signal amplitude is color-coded. Raindrops cause a high number of near-distance detections. The signals with higher intensities are reflected by the quay. The data set is shown again in Fig. 5 in greater detail, particularly the points with high amplitudes.

measurements per second. The reason for this is to accumulate more data points as input for the processing. Obstacles can be expected to reflect signals continuously over this small time interval of 1 s while scattered signals can be less consistent over time. According to the Guidelines for Autonomus Shipping by Bureau Veritas [19], the maximum recommended data transmission latency for Remote Control, Radar Images and Telemetry is 1 s. Thus, the time range over which 1D FMCW radar data are accumulated for processing in our work complies with this recommendation.

Regardless of the accumulation, new processed data are available every 0.1 s. Raw data are collected in a queue covering 1 s and every time new raw data are available, the data with the least recent timestamp are omitted from the queue while new data are added.

A. Data Filtering

Prior to clustering, our applied approach includes a two-step data filtering. In the initial filtering step, a lower threshold on the signal amplitude A and an upper limit on the radial velocity v_{rad} is set. All data points passing these criteria, i.e. for which

$$A > A_{\text{min}} \wedge v_{\text{rad}} < v_{\text{rad,max}} \tag{1}$$

are then in a second step filtered according to their number of neighboring points N within a certain radius r_{search}, i.e.

$$N(r_{\text{search}}) > N_{\text{min}} \tag{2}$$

This combined filtering and clustering approach is adopted from [14] with some modifications, e.g. adding the signal amplitude criterion. The latter aims at filtering out signals from targets with a low reflectivity like raindrops. Fig. 4 shows radar distances plotted over time for an example data set recorded during rain. Data are recorded by the sensor mounted at the side of our research boat (see Fig. 2). The reflections from the quay wall appear in the second half of the plot at a distance of ~ 7 m and have higher signal amplitudes than the near-distance rain reflections, which makes them identifiable as the green and yellow data points. The figure also shows that the data point density is lower in many cases for the disturbing rain signals than for relevant signals. This motivates the density-based filtering. The idea behind the maximum radial velocity threshold is that our work focuses on collision risk assessment with static port infrastructure. Thus, radial velocities of relevant objects are constrained by the speed of the research boat.

B. Data Clustering

After filtering, density-based clustering is applied to the radar distances. As mentioned before, the performance of DBSCAN, HDBSCAN and OPTICS is compared. Only the spatial distance of data points is considered in forming the clusters, i.e. the temporal distance is disregarded. As stated above, data accumulated over 1 s is processed together. Since chances are high that there is more than one obstacle in the field of view (FOV) of a radar sensor, the two largest clusters formed are considered in each processing step. An overall distance is calculated for both of them as a weighted mean value. Finally, the distance to the closer cluster between the largest two is selected as the final radar distance since it is more relevant for collision avoidance. To calculate the average distance of a cluster, each member target is weighted by a factor that includes its signal amplitude A_i, the distance value d_i itself and the time difference between present time t_1 and time of the respective measurement t_i. The equation for the weighting factor is

$$w = \sum_{i=1}^{N} (c_1 A_i + c_2/d_i + c_3/(t_i - t_1 + 0.1)) \tag{3}$$

where N is the number of data points in the respective processing step, i.e. the number of data points recorded within the time interval $[t_1 - 1\,\text{s}, t_1]$. t_1 is the time for which an overall distance value is to be determined. A factor of 0.1 is added to the denominator to shift the root. The coefficients c_i were selected empirically, and are listed in Table I. The ideas behind those three factors are that signals with stronger amplitudes have the highest probability to correspond to actual obstacles. Further, closer distances imply a higher collision risk. And last but not least, the most recent measurement is weighted stronger than older ones to reduce the error introduced by processing data in aggregations of 1 s in case the distance changes considerably over this time interval.

IV. Evaluation

A. Ground truth reference and metrics

The final radar distances were compared to a DGPS-based ground truth in order to assess whether our data processing

Table I
COEFFICIENTS FOR THE WEIGHTING FACTOR OF THE AVERAGE CLUSTER DISTANCE CALCULATION (SEE EQ. 3).

coefficient	c_1	c_2	c_3
value	1	1000	0.5

yields a valid distance.

To get a general overview of the data processing performance across all data sets, obtaining one single evaluation index per data set is beneficial. Therefore, the mean deviation from ground truth for all processed distance values of a specific maneuver was calculated, i.e.

$$\overline{|d_{\text{final}} - d_{\text{GPS}}|} = \sum_{i=1}^{N_{\text{clustered}}} \frac{|d_{\text{final},i} - d_{\text{GPS},i}|}{N_{\text{clustered}}} \tag{4}$$

Here, $N_{\text{clustered}}$ is the total number of distance values obtained for a data set after filtering and clustering, $d_{\text{final},i}$ the i-th radar distance value resulting from data processing and $d_{\text{GPS},i}$ the DGPS based ground truth distance of the boat to the quay wall at the time of the radar measurement resulting in $d_{\text{final},i}$.

Besides matching the ground truth distance, another key aspect of the data processing is to provide one single distance value for each time step where a relevant obstacle is in the FOV of the sensor. Selecting the parameters for filtering and clustering too restrictively can result in a small number of clusters. This implies large time intervals during which no final distance value is obtained although there is an obstacle nearby. This would render the processed data unusable for collision risk estimation. Therefore, a second evaluation metric introduced is the data point frequency,

$$\nu_{\text{DP}} = N_{\text{data points}}/\Delta t \tag{5}$$

where Δt is inserted in $\frac{1}{10}$ seconds since this is the data point frequency of the raw radar data.

Both evaluation metrics were compared for the raw distances, filtered distances and those resulting from data processing.

B. Experimental setup

Our study utilized RMS 1000 FMWC radar sensors from SICK, configured with a horizontal opening angle of $\pm 10°$. Their vertical opening angle is fixed to $\pm 4°$. The operating range is specified to be between 0.4 m and 100 m and the frequency is modulated linearly between 61 GHz and 61.5 GHz. One measurement cycle takes 100 ms, thus 10 measurements are completed each second. The output which forms the basis for our data processing consists of radar targets characterized by a distance, radial velocity and signal amplitude. Given the fact that 1D radar sensors are utilized, information on the azimuth angle of the target is not available.

Besides rain, also wind speed influences the quality of the radar data as an environmental factor since wind causes waves and therefore increases the probability for detecting radar reflections from the water surface. For this reason, wind speed during sea trials was measured with a wind sensor mounted on top of our research boat.

In order to calculate the ground truth, the quay wall's position was sourced from electronic nautical charts provided by the *Bundesamt für Seeschifffahrt und Hydrographie* (BSH), accessed through a SevenCs WMS chart server. The position of the research boat is determined via differential GPS measurements using a Saab R5 Navigation system. All radar and position data were recorded with timestamps which is an important precondition for assigning the correct ground truth to each final radar distance value.

Distance offsets corresponding to the position differences between the radar sensors and the DGPS were considered when comparing d_{GPS} and d_{final}, as illustrated in Fig. 2. Values were derived from the mechanical drawing of our research boat.

Since both radar distance and DGPS position measurements are subject to uncertainties, it is important to consider their accuracy in order to interpret the ground truth deviations in a meaningful way. The systematic uncertainty of a single radar measurement is 0.1 m according to manufacturer specifications. Additionally, the radar sensors were operated with a horizontal opening angle of $\pm 10°$. This results in an uncertainty of $\approx 0.015d$ for a measured distance d. When the sensor is facing a plane object oriented perpendicular to its line of sight at a given distance d, the distance for a detection at angle $\pm 10°$ is $\approx 0.015d$ larger than the one at $0°$. Thus, e.g. at a distance of 10 m, which is roughly the point where the port side turn was performed during the maneuvers (see Sect. IV-C), the distance uncertainty induced by the horizontal opening angle of the sensor is ≈ 0.15 m. If the sensor does not face the quay wall perpendicularly, the uncertainty is larger. In this case, the comparison to the DGPS-based ground truth is not valid since the DGPS-based distance is by definition the shortest way between boat and quay wall, i.e. the perpendicular case.

In addition to uncertainties in the radar distance measurements, those of the DGPS-based ship position have to be considered. The DGPS data used by us provide error estimates in longitude, $\Delta\lambda$, and in latitude, $\Delta\phi$, for each position measurement. The overall position error was calculated as $\sqrt{(\Delta\lambda)^2 + (\Delta\phi)^2}$. A maximum of ≈ 0.5 m was found for all data sets under consideration.

The overall uncertainty range is the sum of all aforementioned contributions and can therefore be estimated as 0.75 m. An unknown factor in this consideration is the accuracy of the quay wall position that was extracted from the BSH nautical charts. The quay wall used for the evaluation more closely resembles a green bank than a vertical wall. This implies an additional unknown inaccuracy because the area of the quay producing the strongest radar reflections is not necessarily the same that is declared as shore line in the nautical chart.

Therefore, the uncertainty range around the quay wall position was assumed to be ± 2 m, extending the value of 0.75 m that is induced by radar distance and DGPS position uncertainties. A deviation of the final radar distances to ground

Table II

PROPERTIES OF THE DATA SETS USED FOR THE EVALUATION. FOR THE SOG AND WIND SPEED, THE MEAN VALUES AND STANDARD DEVIATIONS OF ALL MEASUREMENTS TAKEN DURING THE RESPECTIVE MANEUVER ARE LISTED. THE BOTTOM LINE CHARACTERIZES THE BACKGROUND BEHIND THE QUAY AT THE LOCATION WHERE THE RESPECTIVE MANEUVERS WHERE CARRIED OUT (SEE TEXT FOR FURTHER DETAILS).

data set no.	1	2	3	4	5	6	7	8	9	10
duration [s]	56	29	36	39	84	119	135	98	81	99
SOG [kt]	5.0±0.4	4.9±0.4	5.0±0.4	4.9±0.3	2.9±0.4	2.1±0.4	1.8±0.3	5.0±0.6	4.8±0.7	5.1±0.7
wind speed [kt]	10.5±1.5	10.6±2.4	9.2±1.5	9.6±1.4	4.6±2.3	4.8±2.5	4.7±1.3	4.3±3.7	6.3±3.6	4.4±4.3
weather conditions	rain				dry			dry		
background objects	factory hall				–			factory hall		

truth that is within this range of $\pm 2\,\mathrm{m}$ then implies a valid radar distance.

C. Field Tests and data set

The radar data for the evaluation was recorded within the physical testbed of the eMaritime Integrated Reference (eMIR) Platform [2] [20]. To record radar data in the field, our research vessel *Sally* was used. In order to evaluate the chosen method, data from a radar sensor mounted at the bow of the research boat (see Fig. 1) with line of sight parallel to the surge direction and from a second sensor at the starboard side with line of sight perpendicular to the surge direction was considered. In total 10 maneuvers were carried out during which the vessel approached the quay wall head-on, performed a 90° port side turn and then moved parallel to the quay. The data was recorded during two trial runs at Emden Harbor on August 2nd, 2023 (data sets 1 to 4) and August 29th, 2023 (data sets 5 to 10). The weather conditions were considerably worse for the test trial on August 2nd, characterized by rain and an average wind speed of 10.0 m/s as compared to August 29th with dry weather and an average wind speed of 4.9 m/s.

Table II gives an overview of the maneuver durations, average speed over ground and wind speed for all data sets.

The manuevers of data sets 1-4 and 8-10 were carried out at the same location within our trial area, which is characterized by a factory hall behind the quay. Maneuvers 8-10 were carried out at a slightly different location with less prominent background objects on the shore.

D. Filtering parameter selection

The results of the filtering and clustering processes strongly depend on the selection of the respective parameters. Table III gives an overview of the applied values. The considerations leading to the selection of these values are described in the following.

The parameters of the filtering algorithm were selected based on a visual inspection of our data sets. The challenge in selecting the filtering parameters is finding a trade-off between removing as many irrelevant detections as possible and not dismissing a considerable amount of relevant detections. The maritime environment further complicates this task since measurements are subject to bad weather conditions like rain or heavy wind that churns up the water surface causing more wave reflections. Since always 10 measurements are processed together, the first filtering parameter, i.e. the minimum number of neighbouring points, was set to $N_{\min} = 10$. This can be interpreted as the expectation that an obstacle causes on average at least one signal per measurement cycle with an amplitude $> A_{\min}$. For the search radius r, several values in the range [0.5, 2.5] have been tested and a value of 1.5 was selected after sampling plots of the filtered data. This value showed the best trade-off of filtering out as many unwanted signals as possible while not causing gaps in relevant detections. Fig. 5 shows the effect of filtering with two different r_{search} on an example data set. Plotted are again radar distances over time as in Fig. 4.

The upper limit set on radial velocity of radar targets during filtering is selected based on the maximum speed over ground of our research boat, which is $6\,\mathrm{kt} \approx 3\,\mathrm{m/s}$. A threshold of $v_{\mathrm{rad,max}} = 4\,\mathrm{m/s}$ was established in order to account for possible measurement uncertainties or current and wind influences additionally accelerating the vessel.

The signal amplitude threshold, $A_{\min}$, aims at filtering out scattered signals mostly reflected by the water surface or raindrops. Based on visual inspections of our data, it was set at a value of 10 dB.

E. Clustering parameter selection

The clustering algorithms employed in this study, sourced from Python's *scikit-learn* library, include DBSCAN, HDBSCAN, and OPTICS.

To limit the complexity of the clustering optimization problem, $min\_samples = min\_cluster\_size$ was set for HDBSCAN and OPTICS. Both values were set to a value of 10, based on the same assumption used in the filtering parameter selection: An object relevant for collision avoidance would likely cause at least one reflection per measurement cycle, thus ≥ 10 reflections per second. The ϵ parameter was variable in our evaluation, testing values ranging from 0.5 to 3.0 in steps of 0.5 to identify the optimal setting for our application.

V. RESULTS AND DISCUSSION

A. Quantitative considerations

The evaluation metrics across all data sets and sensors are displayed in Fig. 6. Results for the three clustering algorithms are shown in different colors and varying ϵ values are denoted by distinct markers.

As expected, the number of data points per unit time (Figs. 6(a) and 6(b)) is reduced in both data processing

[2]https://emaritime.de/, accessed 2023-12-08

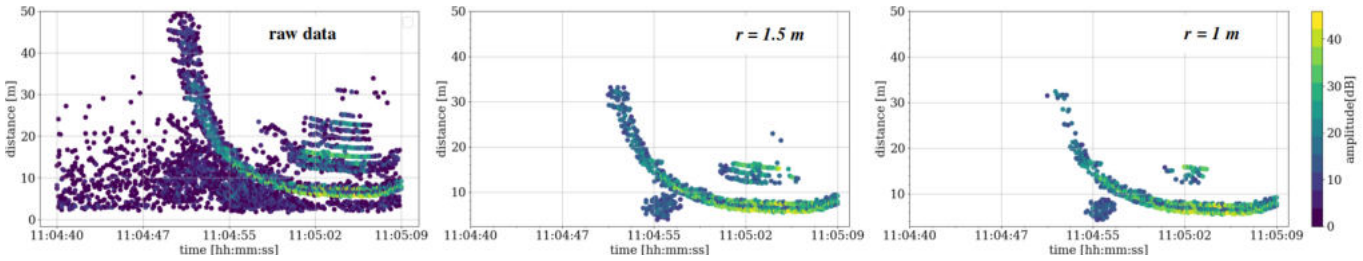

Fig. 5. Example of filtering results with different search distances r for the density-based criterion (see Sect. III-A). The top left panel shows the unfiltered data set recorded by the radar sensor mounted on the right hand side of the research boat. The near-distance signals at timestamp 11:04:55 originate from the water surface. Quay wall signals start at $\sim 30\,m$ and go down to $\sim 7\,$m. When reducing the search distance from $r = 1.5\,$m to $r = 1\,$m, gaps become evident. The larger distances at 11:05:02 originate from background objects behind the quay (see Fig. 2).

Table III
OVERVIEW OF THE VALUES SELECTED FOR FILTERING AND CLUSTERING PARAMETERS. ϵ WAS TREATED AS A FREE PARAMETER IN THE EVALUATION.

	filtering				clustering		
Parameter	A_{min}	$v_{\text{rad,max}}$	r_{search}	N_{min}	*min_samples*	*min_cluster_size*$^{(*)}$	ϵ
Value	10 dB	4 m/s	1.5 m	10	10	10	$\in [0.5, 1, 1.5, 2, 2.5, 3]$ m

(*) only applicable to HDBSCAN and OPTICS

steps, i.e. filtering and clustering. It is less than one for the final distance values which can be explained by the fact that the quay wall is not in the FOV of both sensors during the whole time throughout the maneuver. The front sensor captures it only before the 90° turn and the side sensor only afterwards. Assuming the turn occurs mid-maneuver, a value of approximately $0.5/(0.1\,\text{s})$ is expected for both sensors, which is marked by the black dashed line. It is approximately reached for almost all algorithms and ϵ values, except for DBSCAN and HDBSCAN with $\epsilon = 0.5$ where $N_{\text{datapoints}}/\Delta t$ is considerably smaller for the front sensor (Fig. 6(b)). In these cases, time gaps in the final radar distances occur.

The second metric, namely the mean deviations from ground truth for each maneuver, is plotted in Figs. 6(c) and 6(d). The raw data (indicated by black empty square markers) exhibit considerably larger mean deviations compared to the filtered (empty black triangles) and final distances (colored markers). Overall, differences between the three clustering algorithms are minor. OPTICS with $\epsilon = 0.5$ (denoted by red '+' markers) tends to perform particularly well.

For the side sensor, all data sets show mean deviations below 3 m from the ground truth (Fig. 6(c)). In Sect. IV-B, a valid radar distance range of $\pm 2\,$m around the ground truth was derived. The border of this range is marked by the black dashed line in Figs. 6(c) and 6(d). The largest deviations for the side sensor distances after data processing exceed the derived uncertainty range by less than 1 m. As mentioned before, the uncertainty of the quay wall position cannot be quantified. Taking that into account, the ground truth deviations for the side sensor suggest reasonable accuracy of the processed radar distances for all three clustering algorithms over the whole ϵ range. In contrast, for the front sensor, ground truth deviations are greater than $4\,$m for at least 2 data sets, depending on the choice of clustering algorithm and ϵ (see Fig. 6(d)). This might be attributed to background objects that are reflecting radar signals better than the quay wall. Since only the two largest clusters are considered in each processing step, prominent background objects can lead to an elimination of the quay wall signals in data processing. There is a factory building behind the quay in the area where the maneuvers of data sets 1-4 and 8-10 were carried out. In contrast, the area where maneuvers 5-7 took place exhibits less background objects. Ground truth deviations for the front sensor for the latter maneuvers are within the margin of uncertainty of 2 m. This supports the hypothesis that the larger deviations for the other data sets are related to background objects. The front radar sensor is mounted at the top of the vessel bow, which makes its location higher than that of the side sensors. Therefore, it is more prone to detecting background objects.

B. Qualitative considerations

A qualitative representation of final radar distances and ground truth allows for a more detailed evaluation and the identification of gaps that might result from unfavorable parameter settings. Figs. 7(a) to 7(c) show exemplary plots of data set 1 for DBSCAN with $\epsilon = 1$, HDBSCAN with $\epsilon = 1.5$ and OPTICS with $\epsilon = 0.5$ respectively. The ϵ values were selected based on Figs. 6(a) to 6(d). The ground truth is represented by a black solid line, which is the interpolated representation of DGPS measurements taken with a frequency of $1\,\text{s}^{-1}$. Around time stamp 11:01:53, near-distance reflections from the water surface are observable which form clusters for all three algorithms. However, for OPTICS (Fig. 7(c)) the number of clusters related to this phenomenon is lower than for HDBSCAN or DBSCAN. The reflections coincide with the vessel's 90° turn, suggesting that they might be caused by water being churned up during the maneuver. This hypothesis is supported by a controlled test where radar reflections from the water surface could be induced while the vessel was moored and waves were created with its propulsion system.

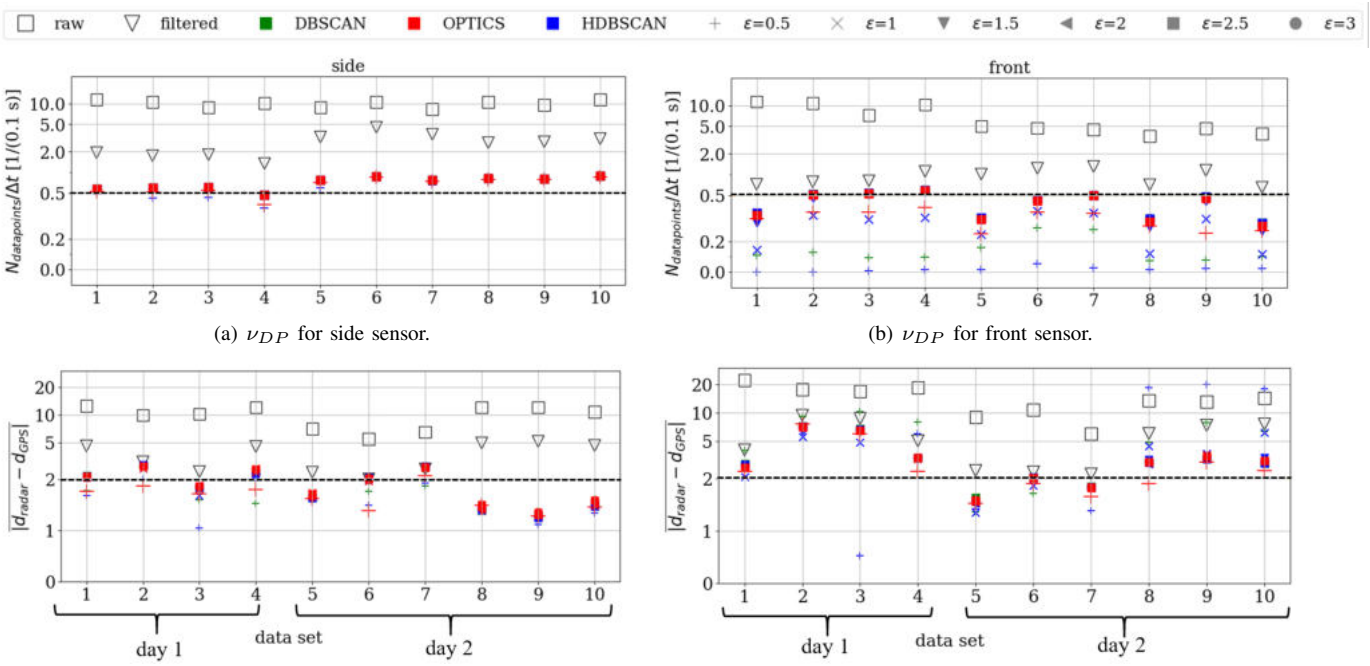

(a) ν_{DP} for side sensor.

(b) ν_{DP} for front sensor.

(c) Ground truth deviations for side sensor.

(d) Ground truth deviations for front sensor.

Fig. 6. Evaluation of distance values was conducted for sensors mounted at the port side ((a), (c)) and bow ((b),(d)) of the research boat, with data set numbers on the $x-$axis (refer to Table II). Upper plots display data point frequency ν_{DP} in $(0.1\,\mathrm{s})^{-1}$, matching the sensor's measurement interval. Lower plots show mean deviations from ground truth distance. Values are plotted with symmetric log $y-$axis scaling and linear labels. Black dashed lines indicate expected values. Black squares and triangles represent raw and filtered data, respectively. Results from DBSCAN, HDBSCAN, and OPTICS are in green, blue, and red, with different markers for various ϵ values.

In order to assess the influence of the 6 DOF vessel motion on the radar data, a second test was conducted where the research boat was excited manually to roll angles up to 5°. This coincides with the maximum roll angles observed during the maneuvers. No reflections from the water surface were observed during the test, suggesting that the state of the water surface has a greater influence on radar data than large roll angles.

Two other things are worth mentioning in Figs. 7(a) to 7(c): Firstly, for the front sensor, some final distances considerably exceed the ground truth. These anomalies either originate from background objects, as previously discussed, or from signals detected at the edge of the FOV. Secondly, there is a temporary increase of ground truth deviations in the moment of the 90° turn right before timestamp 11:04:54. This is caused by both the front and side sensor seeing the quay wall on the edge of their FOV during the turn. Thus, during the turn, there is a short time interval during which none of the sensors measures the correct distance.

C. Feasibility for online application

To assess collision risks with static obstacles during remote control operations, data processing has to be applied in real-time during sea trials. The following considerations are intended to give a rough estimate on the feasibility for online application. We evaluated the processing times for filtering and clustering for data set 1, measuring the duration from inputting raw data to obtaining final radar distances. Processing times increased from DBSCAN to HDBSCAN and OPTICS, with the maximum outlier found for HDBSCAN at 0.13 seconds. In over 90% of cases, all three algorithms processed data in under 0.05 seconds. The sensor's measurement frequency is 10 Hz, thus the data processing is fast enough in a majority of the cases to catch up with new sensor data becoming available.

VI. Conclusion

We presented an approach for 1D FMCW radar data processing in the maritime environment using the clustering algorithms DBSCAN, HDBSCAN, and OPTICS. The data processing results were evaluated against a DGPS-based ground truth using data recorded in a harbor area during sea trials. This approach provides an assessment of the performance of the algorithms under different environmental influences. All three algorithms yielded good results, although care has to be taken when choosing the ϵ parameter. OPTICS with $\epsilon = 0.5$ showed the best performance when filtering out reflections from the water surface. Remaining challenges include a better handling of wave reflections and background objects. The latter is related to the fact that only the two largest clusters are considered in each processing step. Considering more clusters increases the probability of capturing the closest obstacle also in presence of background objects. At the same time, this approach raises the probability that clusters formed by disturbing signals like wave reflections are considered to be obstacles.

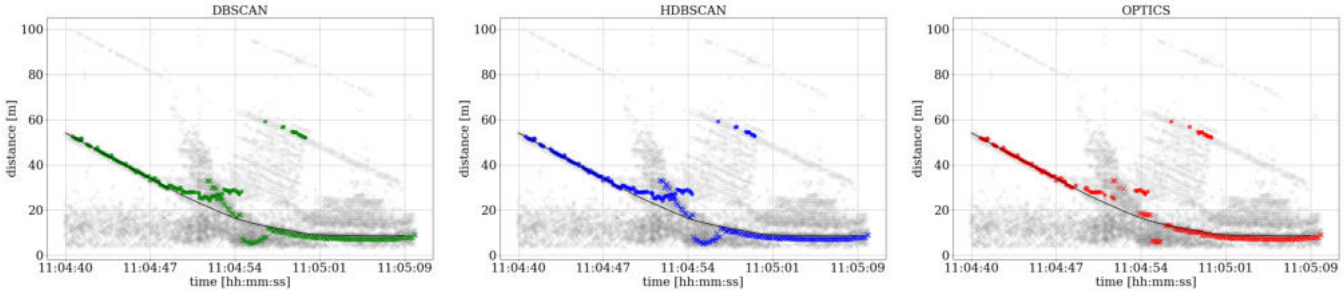

(a) DBSCAN clustering, $\epsilon = 1.0$ (b) HDBSCAN clustering, $\epsilon = 1.5$ (c) OPTICS clustering, $\epsilon = 0.5$

Fig. 7. Distance as a function of time for data set 2 using different clustering algorithms. The black solid line is the interpolated representation of the DGPS-based ground truth distance. Grey markers represent the raw data. Data of both the front sensor (circle markers) and side sensor (cross markers) are plotted. In the first part of the maneuver, the quay wall is in the FOV of the front sensor. Before 11:04:54, the the 90° port side turn takes place, after which the quay wall is in the FOV of the starboard side sensor.

The distance values resulting from our data processing can be used for a safer navigation in remote control operations of surface vessels when distances are displayed in a graphical user interface. Several sensors can be mounted around the vessel to get an omni-directional overview of distances to obstacles. The applicability to a different hardware setup, like a larger vessel, remains to be tested. In general, obstacles have to be of sufficient height, depending on the mounting position of the sensor. An applications case could be detecting the distance to doors and walls when entering a lock. Challenges like reflections from the water surface are expected to be less prominent if sensors are mounted in higher positions like it could be realized for larger vessels.

VII. Conflict of Interests

The authors declare no conflict of interest that could have influenced the results of this work.

VIII. Acknowledgements

The work was conducted within the 'AMISIA - Advanced Port Maintenance: Intelligent, Sustainable and Automated Dredging' project, which is funded by the German Federal Ministry for Digital and Transport (BMDV), in the IHATEC programme under grant ID 19H21003D.

References

[1] International Maritime Organization, *MSC.1-Circ.1638: Outcome Of The Regulatory Scoping Exercise For The Use Of Maritime Autonomous Surface Ships*, Jun. 3, 2021.

[2] A. Danzer, T. Griebel, M. Bach, and K. Dietmayer, "2D Car Detection in Radar Data with PointNets," in *The 2019 IEEE Intelligent Transportation Systems Conference - ITSC*, Piscataway, NJ: IEEE, 2019, pp. 61–66.

[3] M. A. Mutschler, P. A. Scharf, P. Rippl, T. Gessler, T. Walter, and C. Waldschmidt, "River Surface Analysis and Characterization Using FMCW Radar," *IEEE Journal of Selected Topics in Applied Earth Observations and Remote Sensing*, vol. 15, pp. 2493–2502, 2022.

[4] R. Aguiar, L. Bertini, A. Copetti, E. W. G. Clua, L. M. G. Gonçalves, and L. B. Moreira, "Semantic Segmentation and Regions of Interest for Obstacles Detection and Avoidance in Autonomous Surface Vessels," in *2023 Latin American Robotics Symposium (LARS), 2023 Brazilian Symposium on Robotics (SBR), and 2023 Workshop on Robotics in Education (WRE)*, 2023, pp. 403–408.

[5] N.-s. Son and S.-Y. Kim, "On the sea trial test for the validation of an autonomous collision avoidance system of unmanned surface vehicle, ARAGON," in *OCEANS 2018 MTS/IEEE Charleston*, 2018, pp. 1–5.

[6] H. Song, K. Lee, and D. H. Kim, "Obstacle Avoidance System with LiDAR Sensor Based Fuzzy Control for an Autonomous Unmanned Ship," in *2018 Joint 10th International Conference on Soft Computing and Intelligent Systems (SCIS) and 19th International Symposium on Advanced Intelligent Systems (ISIS)*, 2018, pp. 718–722.

[7] M. S. A. b. M. Rafi, W. Sediono, and Z. b. Z. Abidin, "Radar-Based Collision Avoidance on Unmanned Surface Vehicles (USV)," in *2022 IEEE 9th International Conference on Underwater System Technology: Theory and Applications (USYS)*, 2022, pp. 1–7.

[8] A. Venon, Y. Dupuis, P. Vasseur, and P. Merriaux, "Millimeter Wave FMCW RADARs for Perception, Recognition and Localization in Automotive Applications: A Survey," *IEEE Transactions on Intelligent Vehicles*, vol. 7, no. 3, pp. 533–555, 2022.

[9] D. de Martini, M. Gadd, and P. Newman, "kRadar++: Coarse-to-Fine FMCW Scanning Radar Localisation," *Sensors (Basel, Switzerland)*, vol. 20, no. 21, 2020.

[10] S. Rudys, A. Laučys, D. Udris, R. Pomarnacki, and D. Bručas, "Functionality Investigation of the UAV Arranged FMCW Solid-State Marine Radar," *Journal of Marine Science and Engineering*, vol. 9, no. 8, p. 887, 2021.

[11] A. L. Merlo, "Automotive radar for the prevention of collisions," *IEEE Trans. Ind. Electron. Control Instrum.*, vol. 11, no. 1, pp. 1–6, 1964.

[12] C. Waldschmidt, J. Hasch, and W. Menzel, "Automotive Radar — From First Efforts to Future Systems," *IEEE Journal of Microwaves*, vol. 1, no. 1, pp. 135–148, 2021.

[13] S. Lim, S. Lee, and S.-C. Kim, "clustering of detected targets using dbscan in automotive radar systems."

[14] N. Scheiner, N. Appenrodt, J. Dickmann, and B. Sick, "A Multi-Stage Clustering Framework for Automotive Radar Data," in *2019 IEEE Intelligent Transportation Systems Conference (ITSC)*, IEEE, 2019.

[15] O. Schumann, J. Lombacher, M. Hahn, C. Wohler, and J. Dickmann, "Scene Understanding With Automotive Radar," *IEEE Transactions on Intelligent Vehicles*, vol. 5, no. 2, pp. 188–203, 2020.

[16] M. Ester, H.-P. Kriegel, J. Sander, and X. Xu, "A Density-Based Algorithm for Discovering Clusters in Large Spatial Databases with Noise," in *Proceedings of the Second International Conference on Knowledge Discovery and Data Mining*, ser. KDD'96, AAAI Press, 1996, pp. 226–231.

[17] R. J. G. B. Campello, D. Moulavi, and J. Sander, "Density-Based Clustering Based on Hierarchical Density Estimates," in *Advances in knowledge discovery and data mining*, ser. Lecture notes in computer science Lecture notes in artificial intelligence, D. Hutchison, T. Kanade, J. Kittler, *et al.*, Eds., vol. 7819, Berlin: Springer, 2013, pp. 160–172.

[18] M. Ankerst, M. M. Breunig, H.-P. Kriegel, and J. Sander, "OPTICS," *ACM SIGMOD Record*, vol. 28, no. 2, pp. 49–60, 1999.

[19] "Guidelines for Autonomous Shipping, NI 641 DT R01 E," Bureau Veritas, Tech. Rep., 2019.

[20] N. Rüssmeier, A. Lamm, and A. Hahn, "A generic testbed for simulation and physical-based testing of maritime cyber-physical system of systems," *Journal of Physics: Conference Series*, vol. 1357, no. 1, p. 012 025, Oct. 1, 2019.